Microscale multiple scattering of coherent surface acoustic wave packets probed with gigahertz time-reversal acoustics

V. Tournat,* D. M. Profunser, E. Muramoto, and O. Matsuda
Department of Applied Physics, Graduate School of Engineering, Hokkaido University, Sapporo 060-8628, Japan

T. Takezaki and S. Sueoka
Graduate School of Information Science, Hokkaido University, Sapporo 060-8628, Japan

O. B. Wright†
Department of Applied Physics, Graduate School of Engineering, Hokkaido University, Sapporo 060-8628, Japan
(Received 26 April 2006; published 15 August 2006)

The multiple scattering of coherent surface acoustic wave packets in a microstructure is studied using an ultrafast optical technique. By recording a set of acoustic transfer functions, we show that it is possible to implement time-reversal acoustics and refocus the wave packets up to the GHz range, two orders of magnitude higher than usual. Many applications in time-reversal acoustics are thus transposable to correspondingly smaller structures, opening the way to efficient nondestructive characterization and manipulation of multiple scattering on the microscale.

DOI: 10.1103/PhysRevE.74.026604 PACS number(s): 43.35.+d, 42.25.Dd, 42.25.Fx, 78.20.Hp

By electronically time reversing and playing back a recorded acoustic wave in a scattering medium, a pulsed-sound field can be made to refocus at the original source position [1]. The time-reversal process, equivalent to a phase conjugation operation in the frequency domain, has been vigorously investigated not only in acoustics but also in fields such as optics or terahertz radiation [2,3]. Such work in fact has ramifications in any field involving wave propagation in a multiple-scattering environment—be it quantum or classical, and irrespective of whether the system is acoustic, optic, or electronic—and involves a diverse range of phenomena such as coherent backscattering or wave localization [4]. In the time domain, however, it is particularly in acoustics that so many practical applications have arisen. Time-reversal acoustics (TRA) at very low acoustic frequencies in seismology [5], at audio frequencies in room acoustics and underwater communications [6,7], and at ultrasonic frequencies (100 kHz–10 MHz) in nondestructive evaluation [8] has allowed spatial resolutions down to millimeter order.

In TRA an acoustic pulse is first locally emitted in a scattering medium and detected by a set of receivers. The receiver signals, termed the codas, are then electronically time reversed. In a final step, each time-reversed coda is played back by its corresponding receiver, and the acoustic field spatiotemporally refocuses at the initial source location. By studying the fidelity of this refocusing, the multiple-scattering medium can be characterized [9].

The properties of TRA systems are best studied when the complete acoustic field can be visualized: hence the interest in imaging the time reversal of surface acoustic waves (SAW's) and plate waves in applications such as characterizing chaotic cavities [10], detecting subsurface defects [11], or localizing contacts on a surface [12]. However, the restriction of TRA to millimeter length scales has precluded the detailed study of multiple scattering in microscopically inhomogeneous samples such as polycrystals, microporous media, metamaterials, or phononic crystals with wide applications in GHz acoustic transduction and absorption.

Here we extend TRA up to ~1 GHz with an ultrafast optoacoustic technique. We record the multiple scattering of SAW's in two spatial dimensions in an array of tiny holes, and show how it is thereby possible to apply most of the existing TRA techniques to multiple scattering in microstructures.

Our sample, shown schematically in Fig. 1(a), consists of a 4×4 array of holes of diameter 8 μm, separation 12.5 μm, and depth ~10 μm. These are fabricated by a wet etching process in a silicon (100) substrate of thickness 0.55 mm. A chromium film of thickness 440 nm, sputtered on top to improve the optoacoustic transduction, introduces some SAW velocity dispersion [13,14]. The small number of holes between the source and detection points, also shown, produce a multiple-scattering geometry while avoiding significant effects arising from the periodicity [15]. (This structure does not exhibit a phononic band gap [16].)

The SAW are generated thermoelastically and nondestructively with ultrashort laser pulses, termed pump pulses, of wavelength 405 nm, duration ~1 ps, repetition rate 76 MHz, and pulse energy ~0.3 nJ. Pump-pulse focusing to a spot radius ~1 μm [13,19] produces broadband surface acoustic wave packets with an omnidirectional wave vector distribution, frequencies 100 MHz to 1 GHz, and acoustic wavelengths 4–40 μm (for a SAW phase velocity ~4000 ms^{-1}) [17]. Optical phase changes ($\sim10^{-4}$) arising from surface motion are spatiotemporally recorded in a Sagnac interferometer [19], making use of two delayed probe pulses of wavelength 810 nm at an interval of 330 ps and focused to a spot radius ~1 μm (derived from the same laser as the

*Present address: Laboratoire d'Acoustique de l'Université du Maine, UMR-CNRS 6613, Université du Maine, Av. Olivier Messiaen, 72085 Le Mans, cedex 9, France.
†Electronic address: assp@kino-ap.eng.hokudai.ac.jp

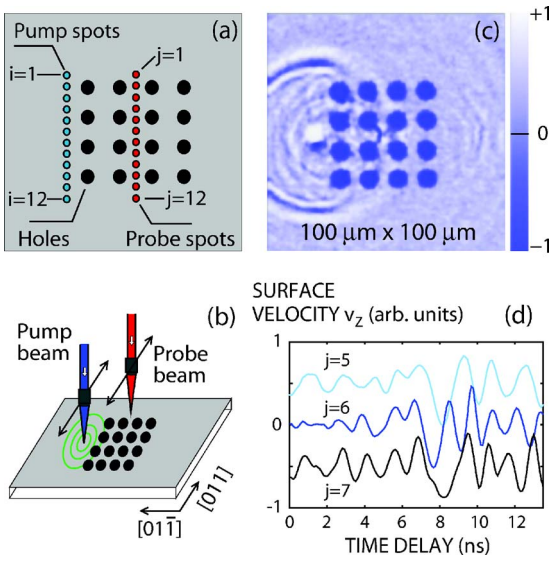

FIG. 1. (Color online) (a) Diagram of the sample. (b) Schematic diagram of the optical illumination geometry, showing the scanning directions for TRA. (c) SAW image of the sample with the source at $i=6$ (with superimposed reflectance image). White corresponds to $v_z>0$. (d) SAW codas ($\propto v_z$), shifted vertically for clarity, recorded at locations $j=5-7$ with the source at $i=6$ [see (a)].

pump). This setup, shown schematically in Fig. 1(b), permits horizontal and vertical spatial resolutions ~ 1 μm and ~ 0.03 pm (at 5 Hz acquisition bandwidth), and a temporal resolution ~ 50 ps here.

Acoustic scattering is evident in a typical SAW image for a fixed pump-probe delay time ($t \approx 7$ ns), shown in Fig. 1(c) (for a ~ 300 Hz acquisition bandwidth). This is a map of the optical phase difference $\delta\phi$ between the two probe pulses, effectively proportional to the time derivative of the out-of-plane surface displacement u_z ($\delta\phi \propto v_z = \partial u_z / \partial t$). Ripples caused by the multiply-scattered surface acoustic wave packets are clearly visible.

To quantify the TRA process in our experiment, we denote the impulse response function for sound generation at the pump spot location by $E(t)$, and the optical pump pulse intensity envelope variation by $p(t)$. The acoustic signal ($\propto v_z$) at the pump spot location is thus given by $e(t)=E(t) \otimes p(t)$, where $\otimes$ is the convolution operator. Since the duration of $p(t)$ (~ 1 ps) is very short compared to $E(t)$ (~ 1 ns), then $e(t) \simeq E(t)$. When this surface disturbance propagates between two points denoted by the in-plane position vectors $\mathbf{r}_i$ and $\mathbf{r}_j$, it is modified according to the transfer function $h_{ij}(t)$ [related to the Green's function $G(\mathbf{r}_i, \mathbf{r}_j, t)$, where t is a time difference], assuming that the medium is linear. The acoustic coda received at j by emission at i will therefore have the standard form $s_{ij}(t)=e(t) \otimes h_{ij}(t)$.

In conventional TRA the database of codas $s_{ij}(t)$ is electronically time reversed to give $s_{ij}(-t)=e(-t) \otimes h_{ij}(-t)$, and these are played back by N transducers at the points j of the coda reception. The contribution to the signal received at any point k arising from a transducer at j can be written as $x_{kj}(t)=s_{ij}(-t) \otimes e(t) \otimes h_{jk}(t)$. For a source initially at i, the total signal played back to point k is therefore given by

$$x_k(t) = e(t) \otimes e(-t) \otimes \sum_{j=1}^{N} h_{kj}(t) \otimes h_{ij}(-t), \qquad (1)$$

where t here is defined for the playback stage and we have exploited the spatial reciprocity of the transfer function ($h_{ji}=h_{ij}$). The convolution operation between a function and its time-reversed counterpart is an autocorrelation. It follows that if the set h_{ij} are uncorrelated, as in a strongly scattering medium, the sum in Eq. (1) for $k=i$ tends to a spatial and temporal δ function (within the constraints set by diffraction), implying a refocusing of the wave packet to point i [9]. In particular, $x_i(t)$ tends to $e(t) \otimes e(-t)$, which has a similar duration to $e(t)$; that the time reversal is imperfect—$x_i(t)$ does not tend to $e(-t)$—is the inescapable result of the use of localized playback points that radiate acoustic fields in all in-plane directions.

For the time scales in our experiment, however, we run into a difficulty: with present spatial-light-modulator technology, for example, optical ultrashort-pulse intensity profiles can only be controlled for a ~ 20 ps duration, rather than the ~ 10 ns we require for executing the playback [20,21]. The method we propose here to complete the TRA process relies on the incorporation of a computational step to evaluate the time-reversed signal $x_{kj}(t)$ from the measured s_{ij} instead of by physically reemitting acoustic signals [8,15]: we therefore (1) record the codas $s_{ij}(t)$ at j for source locations i, (2) numerically time reverse the codas to give $s_{ij}(-t)$, and (3) numerically reemit this signal at j to one of the original source locations (labeled by k) to obtain the matrix $x_{kj}(t)=s_{kj}(t) \otimes s_{ij}(-t)$. This can be summed over j to give $x_k(t)$ for a chosen source i.

We have recorded the codas $s_{ij}(t)$ over two parallel rows of 12 pump (i) and 12 probe (j) spots with a 5 μm spot separation and a 30 μm row separation [see Fig. 1(a)], representing a total of 144 recordings. These rows straddle two rows of microholes, ensuring the production of a complex acoustic field at any j of forward- and back-scattered SAW's. Codas $\delta\phi(t) \propto v_z$ obtained for $i=6$ and $j=5,6,7$ are shown in Fig. 1(d). We obtain a good peak-signal to noise ratio $\sim 200:1$ (at ~ 5 Hz acquisition bandwidth). The signal is periodic in the laser repetition time $T=13.1$ ns (equivalent to a 4 m optical delay). The response within T is made up of a sum of contributions from a succession of pump laser pulses. A finite coda normally imposes a limitation on TRA. However, in our case all available information lies within T. One can in fact demonstrate analytically that, in the case of a periodic signal, performing an autocorrelation operation over T gives exactly the same result as that obtained from the (scaled value of the) multiple-period signal.

In Fig. 2 we plot 12 time-reversed signals calculated from the experimental codas corresponding to SAW's initially emitted at $i=6$ and detected at $j=1-12$. An equivalent image plot is shown in Fig. 3(a). Each signal $x_k(t)$ represents the result of time reversal and reemission by the array of 12 "transducers" labeled by j,

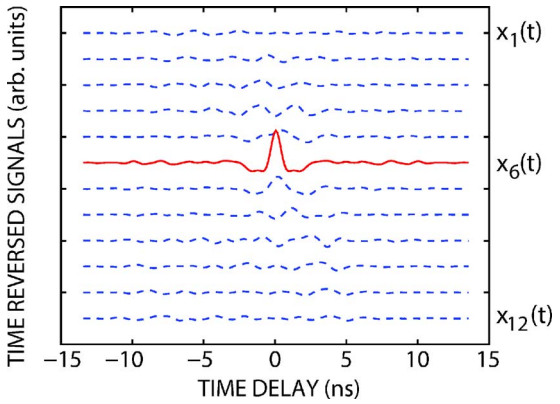

FIG. 2. (Color online) Time-reversed signals $x_k(t)$ at 12 different locations k, shifted vertically for clarity. The initial signal is emitted at $i=6$ (solid line). All 12 values of j are used.

$$x_k(t) = \sum_{j=1}^{12} s_{kj}(t) \otimes s_{6j}(-t). \tag{2}$$

We observe a clear spatial and temporal refocusing at the initial source location $k=i=6$ and at time $t=0$ [18]. The pulse duration there takes the value ~ 1 ns, as determined by $e(t) \otimes e(-t)$. These features are expected when applying the time-reversal operation to a multiple-scattering medium, which effectively acts as a lens [9,10].

To further investigate the spatial refocusing, we plot the directivity pattern, which is the normalized maximum of $x_k(t)$ as a function of k, under different operation conditions in Fig. 4. When all 12 receivers are used for the playback step (solid black line), the directivity pattern has a width of ~ 10 μm. This is of the same order as the dominant acoustic wavelength, indicating an approximately diffraction-limited refocusing in space. This and the observed temporal refocusing indicate that the degree of multiple scattering amply fulfills the criterion for efficient TRA, although an average background level of one-fifth of the peak height remains. However, as the number of receivers used for the playback is decreased, we observe a progressive degradation in the spatial refocusing and an increase in the peak-to-background ratio, as shown in Fig. 4 for the cases of $N=9$, 6, and 1 receivers. With only one receiver, the spatial refocusing is corrupted, as is evident in the space-time plot of Fig. 3(b).

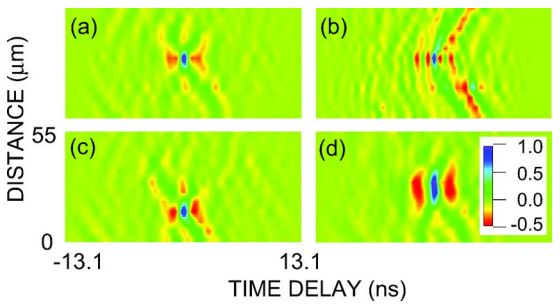

FIG. 3. (Color online) Normalized TRA space-time plots of $x_k(t)$: (a) Source at $i=6$. (b) Only one reemitter, $j=6$, instead of 12. (c) Source at $i=9$. (d) four sources at $i=5-8$.

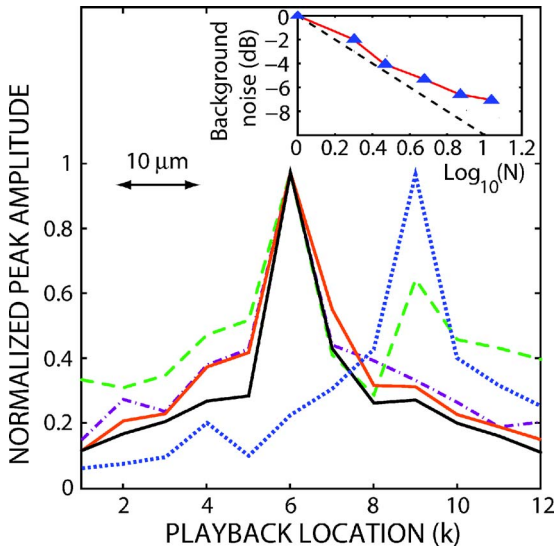

FIG. 4. (Color online) Normalized TRA directivity patterns. Solid black line: initial source location $i=6$ and 12 receivers. Solid gray line (red online): the same using nine receivers ($j=2-10$). Dashed-dotted gray line (purple online): the same using six receivers ($j=4-9$). Dashed line (green online): the same using one receiver ($j=7$). Dotted black line (blue online): initial source location $i=9$ using 12 receivers. Inset: log-log plot of the background noise as a function of the number of receivers N; the dashed line is a $1/\sqrt{N}$ variation.

Such one-channel TRA is known to break down when the length ($L \sim 20$ μm) of scattering medium between the source and receivers is of the same order as the elastic mean-free-path ($l \sim 15$ μm—determined by the hole-to-hole distance), as is the case here [10,22]. One can also note an increasing delay in the signal peak arrival in Fig. 3(b) as $|k-6|$ increases. This is caused by the expected ballistic contribution to the signal that affects the time of the peak of the autocorrelations $s_{kj}(t) \otimes s_{6j}(-t)$ for $k \neq 6$.

The fidelity of the TRA process, as determined by this peak-to-background ratio, is expected to depend on the ratio of incoherent and coherent contributions [to $x_k(t)$] that increases with the degree of multiple scattering and hence with N [22]. We can test this quantitatively by plotting the average background noise against N (obtained by excluding the points $k=5-7$), as shown by the log-log plot in the inset of Fig. 4; the noise decreases a little less rapidly than a $1/\sqrt{N}$ variation (dashed line—expected for random noise). This deviation from $1/\sqrt{N}$, previously observed on millimeter scales for long source-receiver distances ($L \gg l$) and seen here near the opposite limit ($L \sim l$), is caused by correlations in the scattered wave field [22]. Coda wave correlation is a subject of great interest in nondestructive testing and seismology [23–26]. Such correlations allow information on the Green's function to be derived without the need for a controllable acoustic source, opening up applications in imaging, as described, for example, in Ref. [27].

Our 144-coda database allows the arbitrary choice of source location and size. The dotted line in Fig. 4 and the image plot of Fig. 3(c) represent an example for the location $i=9$. We obtain efficient spatiotemporal refocusing at $k=9$.

Figure 3(d) represents an example of an extended source $i=6-9$, again resulting in good spatiotemporal refocusing. This illustrates the robustness of the time-reversal process for our data set.

There are limitations on the accuracy of this high-frequency TRA. As with conventional TRA, frequency-dependent ultrasonic attenuation and mode conversion to bulk waves may cause frequency components to be lost between emission and reception, and these will thus prove impossible to play back. (This is equivalent to the presence in the wave propagation equation of an odd-order differential operator, which disables the time-reversal invariance.) A similar problem exists in the case of any nonlinearity in the propagation or detection processes [28]. For our particular microstructure and excitation levels, SAW attenuation (over ~ 100 μm) or nonlinear propagation (for strains $\sim 10^{-5}$) are expected to be negligible. Losses through mode conversion to bulk waves may be significant, but evidently not enough to prevent efficient refocusing in this experiment. Another crucial parameter is the signal-to-noise ratio. Noise limits the distance over which a SAW can be tracked [owing to the $1/\sqrt{r}$ geometrical "attenuation" in two-dimensions (2D)], but also affects the computed time-reversal process. The autocorrelation of a random (uncorrelated) noise component can produce a fake time-reversal signal, irrespective of the actual transfer function. (Likewise, and counterintuitively, a signal emitted at the source in the form of random noise will refocus to a well-defined pulse.) Here, however, the level of the random noise is too small for this effect to be significant.

The temporal and spatial scales that are attainable with this method should allow microholes, microdots, or microcontacts to be scrutinized. For example, a recent application of TRA for contact detection can be transposed to higher frequencies [12]. Consider a plate containing one emitter and one receiver (i.e., the pump and probe optical pulses), placed at different locations. The relevant transfer function, accounting for the multiple acoustic reflections at the plate boundaries, can be recorded. If a contact is then created on the plate surface, by a local probe tip for instance, this transfer function will be modified. Let us divide the plate in a given number of regions, and record the transfer function when the contact is effective in each region in a database. If a contact is now produced in an unknown region of the plate, the corresponding transfer function is recorded and compared by cross-correlation to each of the functions in the database. The best correlation coefficient provides the contact position to an accuracy of ~ 1 μm. This method should work in practice, although it is admittedly somewhat cumbersome owing to the necessity for optical excitation.

Other transposable TRA applications are iterative techniques that focus on a dominant scatterer [8], the probing of the sensitivity to perturbations [29], or the detection of multiple targets [30]. In these studies one should characterize the multiple-scattering media by experiments on different numbers, arrangements, and types of scatterer to derive quantities such as the elastic mean-free-path l. In the present experiment we are in the regime of weak sound localization for which $k_0 l \approx 10$, where $k_0 = 2\pi/\Lambda$ is the acoustic wave number for the dominant wavelength Λ. But future studies can cover other regimes, possibly including the unexplored region in TRA at the Ioffe-Regel crossover to strong localization at $k_0 l \approx 1$, where interference between multiply scattered paths drastically alters the transport properties [4].

In conclusion, the basic features of TRA in a multiple-scattering medium are shown to be extendable to gigahertz frequencies. This method should allow the nondestructive evaluation of a wide variety of complex microstructures with SAW's, such as GHz waveguides, chaotic acoustic microcavities, or anisotropic crystallites. One can also envisage implementing near-field optics to further extend the frequency of TRA in order to probe multiple acoustic scattering on the nanoscale.

[1] M. Fink, Rep. Prog. Phys. **63**, 1933 (2000).
[2] A. B. Ruffin, J. Van Rudd, J. Decker, J. Sanchez-Palencia, L. Le Hors, J. F. Whitaker, and T. B. Norris, IEEE J. Quantum Electron. **38**, 1110 (2002).
[3] P. Gunter, Phys. Rep. **93**, 199 (1982).
[4] P. Sheng, *Introduction to Wave Scattering, Localization and Mesoscopic Phenomena* (Academic, New York, 1995).
[5] P. M. Norville and W. R. Scott, J. Acoust. Soc. Am. **118**, 375 (2005).
[6] S. Yon, M. Tanter, and M. Fink, J. Acoust. Soc. Am. **113**, 1533 (2003).
[7] W. A. Kuperman, W. S. Hodgekiss, H. C. Song, T. Akal, C. Ferla, and D. R. Jackson, J. Acoust. Soc. Am. **103**, 25 (1998).
[8] C. Prada, S. Manneville, D. Spoliansky, and M. Fink, J. Acoust. Soc. Am. **99**, 2067 (1996).
[9] M. Fink, IEEE Trans. Ultrason. Ferroelectr. Freq. Control **39**, 555 (1992).
[10] C. Draeger and M. Fink, Phys. Rev. Lett. **79**, 407 (1997).
[11] R. K. Ing, M. Fink, and O. Casula, Appl. Phys. Lett. **68**, 161 (1996).
[12] R. K. Ing, N. Quieffin, S. Catheline, and M. Fink, Appl. Phys. Lett. **87**, 204104 (2005).
[13] Y. Sugawara, O. B. Wright, O. Matsuda, M. Takigahira, Y. Tanaka, S. Tamura, and V. E. Gusev, Phys. Rev. Lett. **88**, 185504 (2002).
[14] G. W. Farnell and E. L. Adler, in *Physical Acoustics*, edited by W. P. Mason and R. N. Thurston (Academic, New York, 1972), Vol. 9, p. 35.
[15] A. Tourin, F. Van Der Biest, and M. Fink, Phys. Rev. Lett. **96**, 104301 (2006).
[16] Y. Tanaka and S. Tamura (private communication).
[17] This includes leaky longitudinal and pseudo-SAW modes.
[18] The wings of the autocorrelation function are included on the time axis in Figs. 2 and 3.
[19] T. Tachizaki, T. Muroya, O. Matsuda, Y. Sugawara, and D. H. Hurley, Rev. Sci. Instrum. **77**, 043713 (2006).
[20] A. M. Weiner, J. P. Heritage, and E. M. Kirshner, J. Opt. Soc. Am. B **5**, 1563 (1992).

[21] V. Tournat, O. B. Wright, and O. Matsuda, Phys. Status Solidi C **1**, 2737 (2004).
[22] A. Derode, A. Tourin, and M. Fink, Phys. Rev. E **64**, 036606 (2001).
[23] O. I. Lobkis and R. L. Weaver, J. Acoust. Soc. Am. **110**, 3011 (2001).
[24] R. L. Weaver and O. I. Lobkis, Phys. Rev. Lett. **87**, 134301 (2001).
[25] R. Snieder, Phys. Rev. E **66**, 046615 (2002).
[26] A. Derode, E. Larose, M. Tanter, J. de Rosny, A. Tourin, M. Campillo, and M. Fink, J. Acoust. Soc. Am. **113**, 2973 (2003).
[27] E. Larose, A. Derode, M. Campillo, and M. Fink, J. Appl. Phys. **95**, 8393 (2004).
[28] M. Tanter, J.-L. Thomas, F. Coulouvrat, and M. Fink, Phys. Rev. E **64**, 016602 (2001).
[29] A. Tourin, A. Derode, and M. Fink, Phys. Rev. Lett. **87**, 274301 (2001).
[30] G. Montaldo, M. Tanter, and M. Fink, J. Acoust. Soc. Am. **115**, 776 (2004).